Mining, Metallurgy & Exploration (2022) 39:1073–1086
https://doi.org/10.1007/s42461-022-00594-0

REVIEW

# Estimating Strength of Pillars with Karst Voids in a Room-and-Pillar Limestone Mine

**Aman Soni[1] · Juan J. Monsalve[1] · Richard Bishop[1] · Nino Ripepi[1] · Jonathan G. Baggett[2]**

Received: 19 September 2021 / Accepted: 29 March 2022 / Published online: 21 April 2022


**Abstract**
Underground limestone deposits are prone to karst void formations due to the dissolution of carbonate rocks. These deposits offer permeable conditions to groundwater flow leading to the formation of a network of void spaces or cavities. The cavities can accommodate unconsolidated sediments and groundwater. Interaction of these voids with a prevalent discontinuity network may lead to ground control problems during mining operations. This paper presents a numerical estimation of the effect of karst voids on the strength of pillars in an underground room-and-pillar limestone mine. It is shown that these voids may contribute to a considerable decrease in pillar strength. Mining advances into such formations may lead to a sudden inrush of groundwater or unconsolidated sediments. Apart from posing a safety hazard, this may also disrupt the pre-planned mine operations and design of the headings and pillars. The procedure for estimation of pillar strength using numerical modeling may provide a viable approach to design the future pillars detected with karst voids. Previous studies performed at the case study mine used ground-penetrating radar (GPR) to map the karst boundaries inside the pillar. Apart from the LiDAR scans used to map the discontinuity network around the pillars, some approximations were made to account for the inadequate discontinuity characterization data. Distinct-element modeling (DEM) is used to simulate the presence of voids and discontinuities in the form of discrete fracture networks (DFN). An effort is made to understand the importance of pillar design and dimensions in an underground limestone mine with karst voids to prevent local instability related to pillar failures.

**Keywords** Pillar strength · Pillar design · Karst · 3DEC · DEM · DFN · GPR · Ground control

## 1 Introduction

Over the past decade, underground stone mining operations in limestone deposits have become more common in the eastern USA. Compared to slope stability efforts in surface operations, ground control operations in underground mining are more complicated and require more engineering and training. Currently, there are 110 underground stone mines in the USA majority of which employ room-and-pillar mining methods to extract limestone for crushed stone products (NIOSH, 2021). Despite employing fewer miners than coal mines, stone mines experience a higher number of reportable injuries. Since 1983, about 12% of all the reported injuries in the stone mining industry are because of rock falls from the roof or pillar ribs (MSHA, 2021).

Compared to other rock types, limestone mines have a higher potential to encounter karst voids at some point during their excavation operations. This is due to the prevalent karstic network developed in the limestone rock masses [1]. These cavities are formed over a long time by the dissolution of carbonate rocks and can be unforeseen until encountered due to mining activities. The hindrance of karsts in the mining operations has been well documented by [2]. The disruption of mining operations while encountering karst cavities often requires potential ground control measures beyond the typical scope of a ground control management plan (GCMP) constituted for the mine. Even the rock mass classification schemes, such as the Rock Mass Rating (RMR) from Bieniawski and the Q-system from Barton, do not classify the karst-affected carbonate rock mass, and therefore the analysis of such cases requires geological analysis of the underground conditions [3].

✉ Aman Soni
amansoni@vt.edu

[1] Mining and Minerals Engineering, Virginia Polytechnic Institute & State University, Blacksburg, VA, USA

[2] Rio Tinto Corporation, Salt Lake City, UT, USA

This paper evaluates the stability of a pillar (designated Pillar-X) with the presence of a karst void in an underground limestone mine. The case study mine is a multi-level room-and-pillar underground limestone mine. The pillar in question, i.e., Pillar-X, lies at a depth of about 180 m from the surface. The study discusses the methods which were utilized in determining the karst boundaries inside the suggested Pillar-X, using ground-penetrating radar (GPR). The size of Pillar-X was left to be bigger than the intended pillar dimensions to counter any local instability issue which may have been suspected by the mine management. The mine has experienced ground control issues such as roof and rib failures in the past. The karst cavities, filled with unconsolidated clayey-rock material, may interact with the immediate roof or ribs in the mine drives, or even around a pillar. The interaction is also dominated by the discontinuity network, which is a typical feature of a naturally fractured limestone deposit. Any karst voids which extend beyond the pillar into the roof and floor will also adversely affect the pillar stability. The potential loading issues caused by the extension of voids beyond the pillar and their interaction with the discontinuities are not discussed in this paper. To study the stability of Pillar-X, a 3-dimensional numerical modeling tool 3DEC was used. This software utilizes a finite-difference distinct element method (DEM) to simulate the condition of an underground excavation. The DEM is useful in characterizing the presence of discontinuous media in the rock mass. The pillar model is framed using the rock material and joint properties that were measured by the mine management and confirmed using laboratory testing. LiDAR scans of the pillar were used for discontinuity mapping of the pillar and assessing the different joint sets using Maptek's I-Site point-cloud processing software. Since all of the joints' characteristics cannot be measured inside Pillar-X, a discrete fracture network (DFN) was employed to create a virtual network system which is the closest possible representation to a real-world joint system. Different scenarios were created to account for the irregularities found in the GPR surveys. For each scenario, the pillar model was analyzed for its strength based on a constant compressive velocity applied to it. The analysis characterizes the significant reduction in the pillar strength in the different scenarios, each with increased karst void volume. The paper also discusses the importance of pillar design in the presence of karst cavities to maximize ore extraction as well as maintain local and global stability in a stone mine.

## 2 Background

### 2.1 Case Study Mine

The case-study mine is situated in a region with synclinal Ordovician limestone. The limestone deposit hosts an extensive network of interconnected karst cavities. These cavities are formed over several years due to the dissolution of limestone rock by the flow of groundwater or weak carbonic acid through the vast fracture network of a limestone deposit. The orebody is 30 m thick and dips at approximately 30° towards the southeast as visible from the outcrop. The levels of the mine are connected by a corkscrew ramp. Each level has an east and west section branching off of the corkscrew ramp; at present, each branch contains a footwall and hanging wall tunnel separated by 24.5 m × 24.5 m × 30.5 m rectangular pillars left after complete extraction from the eventual stoping, and tunnels are approximately 8.5-m tall and 14-m wide.

### 2.2 Pillar Location and Geometry

The pillar being analyzed in this paper, named Pillar-X for this study, is shown in Figs. 1 and 2. After the discovery of karst voids in Pillar-X, the stopes around it were not completely excavated, leaving the pillar height to be 9.5 m as opposed to the intended pillar height of 30.5 m after the complete extraction of stope from the adjacent levels. During the initial preparation of the stope around the pillar, the mine workers faced a safety incident of ground collapse from the side-wall which opened up to the karst cavity.

The spillage of wet clay along with the rock boulders did not result in any injuries but it hampered the operations in that region and required additional mucking and rehabilitation of ground support. Figure 3 shows the material collapse in the mine due to the opening up of the karst cavity. The mine management employed temporary ground support measures such as plastic mesh pinned up with steel straps to prevent heading damage due to clayey-rock material and groundwater seepage. Furthermore, grouting was done as a permanent ground control measure to prevent any suspected local instability issues. Figure 4 shows the temporary ground controls measure taken around the pillar.

### 2.3 GPR Investigative Study

Ground-penetrating radar (GPR) surveys could be effective in detecting dielectric boundaries within a solid structure, such as rock mass or concrete pillars [4]. GPR's advantage to map bedrock depth and soil stratigraphy [5] and mapping fractures in gneissic rocks [6] amongst other works has been well renowned. At the case study mine, investigative work was conducted to detect the shape of any karst void(s) in Pillar-X via a dense grid of 3-dimensional GPR survey [4].

The authors used a 3-sq. m tarp marked with gridded survey lines and shot locations. Figure 5 shows the authors surveying the underground case study mine.

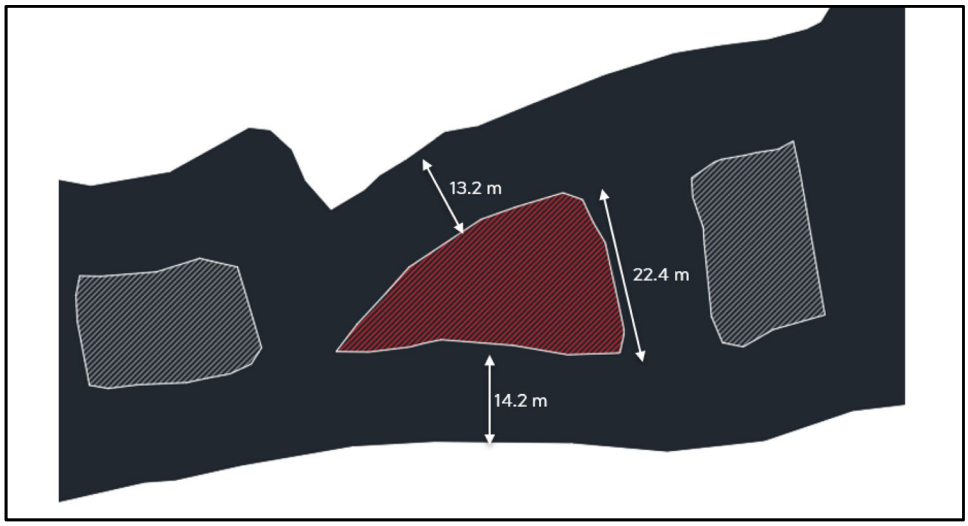


**Fig. 1** Plan view of Pillar-X in the underground mine

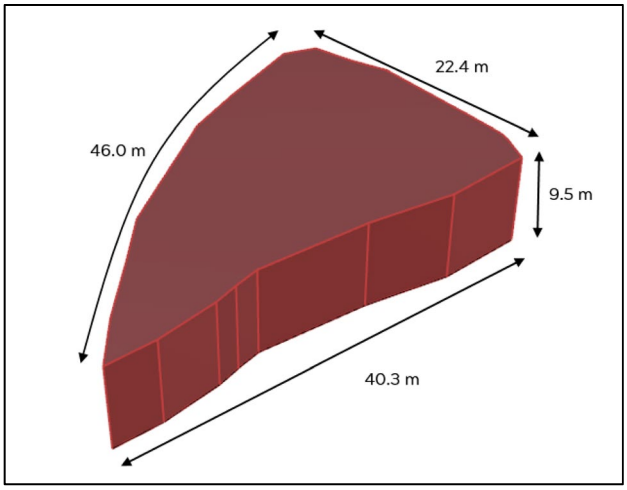


**Fig. 2** Perspective view of Pillar-X in the underground mine

**Fig. 3** Material collapse from karst void in the case study mine (Credits: R. Bishop)

**Fig. 4** Ground support around Pillar-X (Credits: R. Bishop)

The survey was conducted on a total of 8 tarp positions along the ~ 46-m length along one side of Pillar-X. The survey was not extended along the 40.3 m length because of the mesh installed on the collapsed pillar rib to block any inflow of consolidated segments. This prevented any additional data collection for delineating the karst cavity boundaries, considering how groundwater and clayey material attenuate the signals. A 250-MHz antenna was selected by the authors as this frequency showed a penetration depth of greater than 20 m and resolution was favorable to obtain surface reflections. To extract reflection events and ultimately convert these to either points or iso-surfaces, GPR Slice software was used by the authors. The iso-surfaces from all tarp survey grids identified the commonalities and surface trends, as seen in Fig. 6a and b.

The clusters of these iso-surfaces or points were connected to form meshes to produce representative surfaces of the karst void boundary. The plan view of the

**Fig. 5** 3D GPR survey conducted along the Pillar-X

**Fig. 7** Iso-surface meshes created from the reflection points

iso-surface mesh reflection boundary of the karst void inside the pillar is shown in Fig. 7.

Conductive mediums, such as wet clays and water which fill the karst void, highly attenuate the GPR wave energy. Limestone rock is dry, homogenous, and a resistive medium for GPR waves, and is ideal for strongly transmitted and reflected signals [7]. Since the conductive medium inside the void produced reflections, the authors could not propose a closed void volume, which in terms of delineating void boundaries, would be an ideal case. Figure 8 shows a plan view of the approximated karst volume to area projection by the authors [4].

However, the GPR results from this study investigated the surfaces along the pillar sidewalls only. Therefore, there is no information regarding the continuation of discovered cavities above or below the survey window along the pillar. However, accounts from the mining personnel who performed the ground control measures at the site suggest the continuation of void in the immediate roof of the pillar. Also, the physical testing of the void fill material, as indicated by the observed characteristics of reflected radar signals, was not performed. To compensate for the missing information, the karst cavity was assumed to be continuous across the height of the pillar. This will always underestimate the pillar strength as it will possess a larger void volume filled with weak material. Also, different scenarios were considered to include all possibilities for cavity shapes that may affect the pillar strength. These scenarios involved varying the size of karst volume ranging from the approximated volume to a worst-case scenario, where the outer boundaries of the iso-surface reflections were considered with no limestone rock mass in between. These cases are explained further in the sections.

## 3 Distinct Element Modeling in 3DEC

3DEC is a three-dimensional numerical modeling code developed by Itasca Consulting Group [16]. This software is based on the distinct element method (DEM) for simulating the response of the discontinuum network in rock masses such as joints and fractures. The software represents discontinuous media as an assembly of discrete blocks and the discontinuities between them as boundary conditions. For this study, individual blocks are set as deformable material

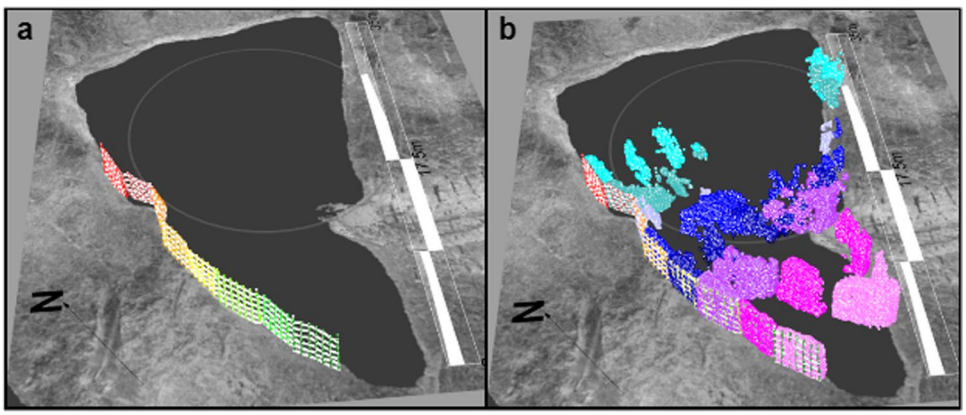


**Fig. 6** **a**, **b** Reflection points obtained from the GPR survey along one side of the pillar [4]

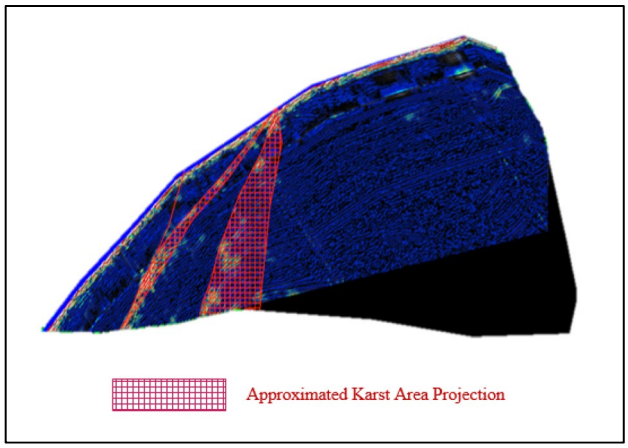


**Fig. 8** Plan view of an approximate karst area projected from the iso-surface meshes [4]

and are meshed as finite different zones. The displacements along the joints and rotation of blocks facilitate us to observe the behavior of the pillar under increasing load.

Pillar strength in stones mines has been studied by many researchers. [8, 9, 11] have suggested methods of estimating the pillar strength and supplemented it with numerical models. [12] addressed the pillar design issues that are typically faced in underground mines. DEM has frequently been used as a tool to analyze rock mass behavior, however, there is a lack of published research on analyzing pillar strength with karst voids detected using underground mining GPR applications.

## 4 Pillar Model Generation

### 4.1 Pillar-X Model Scenarios

For this study, three different scenarios were considered in which the pillar geometry was kept constant. However, the karst void volume was varied to simulate the effect of increasing void volume on pillar strength. The karst voids in the cases were assumed to be empty to underestimate any insignificant support provided by the clayey-rock material present inside the void. The constructed Pillar-X model dimensions were estimated by the LiDAR scans obtained around the pillar. The three scenarios are described in detail below:

i. *Scenario 1* — In this case, the Pillar-X was assumed to be a solid limestone pillar without any karst voids. To assess the effect of karst voids on pillar strength, it is important to model a benchmark pillar strength value. In this case, it was done by simulating the case in which a solid pillar is subjected to increasing compressive stresses until failure is achieved. Figure 9 shows the geometry of the solid pillar. The volume of the original pillar is ~ 5580 cu.m.
ii. *Scenario 2* — In this scenario, the karst voids were created analogous to the iso-surface boundaries as suggested by the GPR study as shown in Fig. 8. The karst voids were assumed to run throughout the height of the pillar. This scenario simulates a most likely case which is suggested by the authors of this paper and also the authors that conducted the GPR study. Figure 10 shows the geometry of the pillar and karst void. The volume of the empty karst void simulated in scenario 2 is roughly 482 cu.m, constituting roughly 9% of the total volume.
iii. *Scenario 3* — In this case, Pillar-X is simulated with the karst voids having the largest volume. It is assumed that the outer boundaries of the GPR iso-surfaces form the shape of the void and there is no hard-rock wedge dividing the void as present in scenario 2. The simulated pillar model of this case is shown in Fig. 11. The karst void in scenario 3 has the largest void volume of about 1009 cu.m, constituting roughly 18% of the total volume.

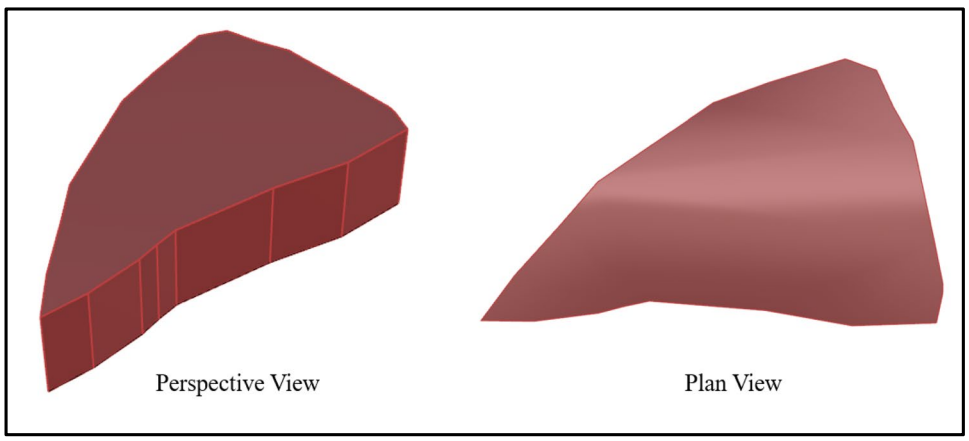


**Fig. 9** Simulated Pillar-X model in scenario 1

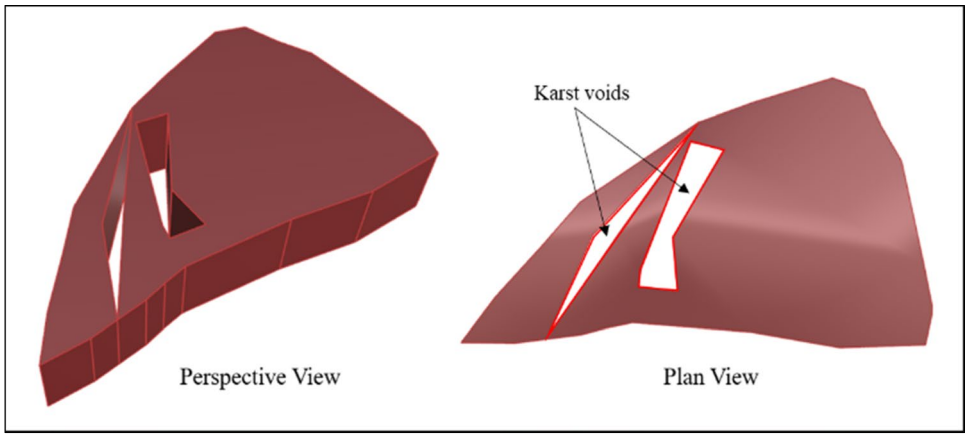


**Fig. 10** Simulated Pillar-X model in scenario 2

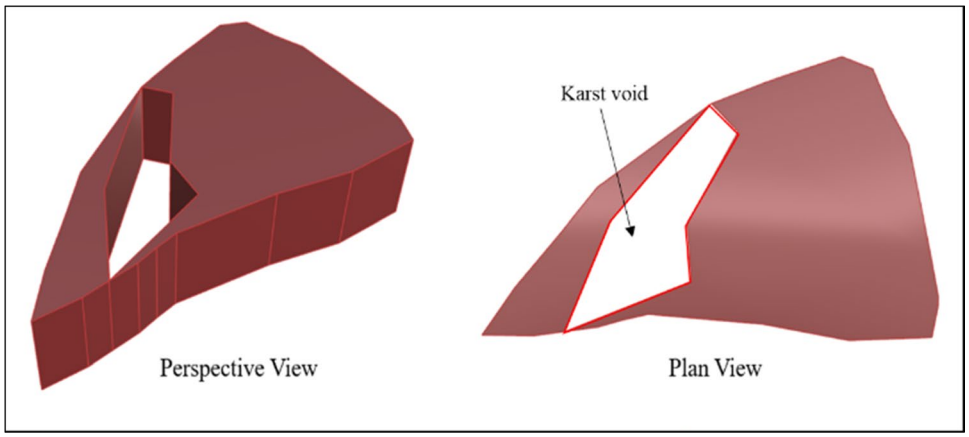


**Fig. 11** Simulated Pillar-X model in scenario 3

## 4.2 Physico-mechanical Properties

The physico-mechanical and geotechnical properties for the rock mass and joints used in the numerical model were measured by the mine management using geotechnical borehole measurements and laboratory testing. The calculated values for joint shear stiffness and joint normal stiffness are based on the work performed by [13, 14]. The properties are listed in Table 1. The lithology of the synclinal Ordovician limestone deposit in the ore body was characterized as Five Oaks limestone [15]. The elastic-isotropic constitutive model is used to represent rock behavior in the numerical model. The authors believe that the strain softening/hardening model could have been the ideal model to simulate the Pillar-X model, but due to the absence of detailed properties, the elastic-isotropic model state was simulated. This constitutive model characterizes the pillar to reflect reversible deformations upon unloading, i.e., the stress–strain laws are linear and path-independent. The Coulomb slip joint constitutive model is assigned to represent the physical response of rock joints. The model simulates the displacement of the discontinuities by weakening cohesive and tensile strength when shear or tensile failure begins [16].

**Table 1** Physico-mechanical properties for rock mass and joints

| Rock mass properties | |
|---|---|
| Density | 2690 kg/m$^3$ |
| Bulk modulus, K | 37.86 GPa |
| Shear modulus, G | 20.57 GPa |
| Poisson's ratio | 0.27 |
| Joint properties [13] | |
| Joint normal stiffness | 300 GPa/m |
| Joint shear stiffness | 30 GPa/m |
| Joint friction angle | 30° |
| Joint cohesion | 0.0 |

## 4.3 Boundary Conditions

For assessing the pillar strength, compressive stresses axially along the $z$-axis to the pillar. Since the pillar is not supported by any material on the sides, no boundary conditions

were applied to the model sides. Fixed boundaries were applied to the top and bottom face of the pillar to prevent any movement and ensure constant stress application with time steps. The load was applied to the pillar model in each scenario using an applied velocity on the top and bottom. It is assumed that only the compressive stress or the vertical stress is being imparted along the axis of the pillar, thus compressing the pillar. No shear stresses are applied on the top and bottom face of the pillar model. The magnitude of the velocity applied was about 0.5 mm/s. Each scenario was cycled until failure of the pillar model in each scenario was observed.

### 4.4 Discontinuity Mapping

An important aspect of the numerical modeling of Pillar-X was to account for the discontinuity network affecting it. Joints play a major role in deciding the strength of a rock mass and detailed knowledge of them would help to simulate accurate conditions. A preliminary investigation was conducted at the case study mine which describes obtaining the LiDAR scans and virtually mapping the discontinuity network around the area from the scans [14]. Maptek I-Site, a point cloud processing and modeling software, was used to extract the discontinuities and different parameters such as joint orientation, fracture density, and size of joints in different joint sets. Figure 12 shows the plan view of the structural mapping performed around Pillar-X. Four discontinuity sets were defined from the mapped discontinuities. Figure 13 shows the process of structural discontinuity mapping in the I-Site.

## 5 Discrete Fracture Network

After sufficient information on the structural features was collected from the LiDAR scans, the data were classified into four joint sets. Extracted data included size information (trace length and area) and orientation information (dip, dip direction, and strike). All this information is used by 3DEC to generate DFNs which simulate a close representation of the geological structures in a rock mass. This fracture network is a set of discrete, planar, finite-size fracture disks, which intersect the model to generate a set of blocks that constitute a simulated jointed rock mass. These disks are created based on statistical data of the joint characteristics, such as orientation, size, and density, measured in the field [17], or in this case, measured virtually from LiDAR point clouds. Table 2 summarizes the statistical data of the joint properties for each joint set used in the modeling study.

One of the important parameters for generating DFNs is fracture density, which is a measure of the spatial frequency of discontinuities in a joint set. This parameter serves as a threshold condition while generating DFNs in 3DEC [10]. For this study, fracture density was defined as the area of fractures per unit volume of the rock mass or $P_{32}$. The DFN model is calibrated using the $P_{32}$ values of the four joint sets measured in the DFNs for the model. Since the fractures per unit volume in the pillar cannot be measured practically through field mapping, $P_{10}$, also known as linear fracture intensity values are measured.

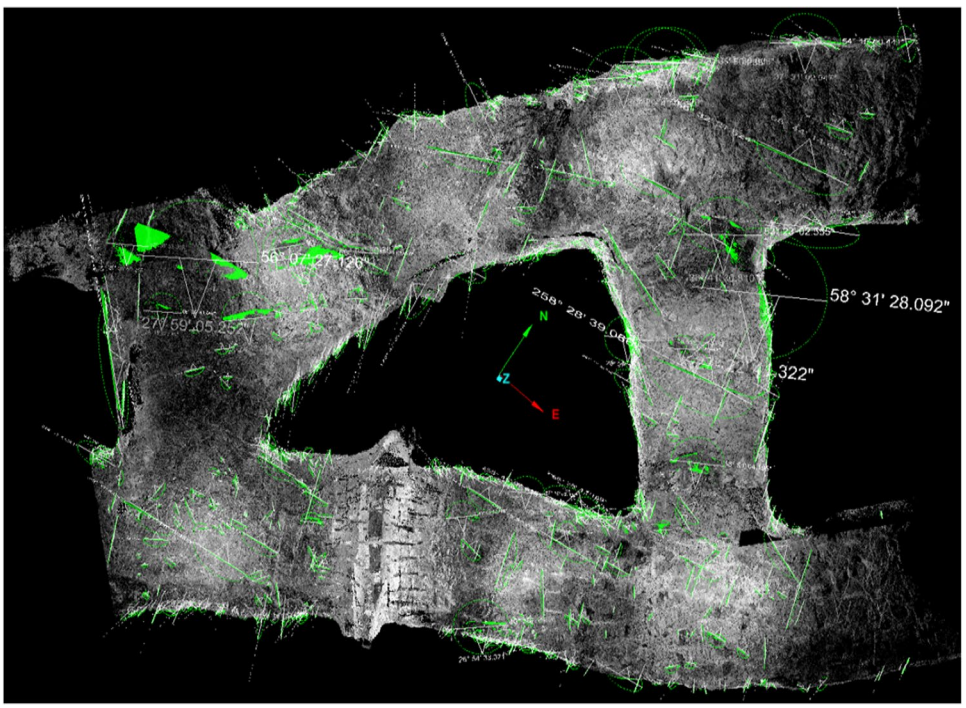


**Fig. 12** Virtual discontinuity mapping from LiDAR scans around the Pillar-X [14]

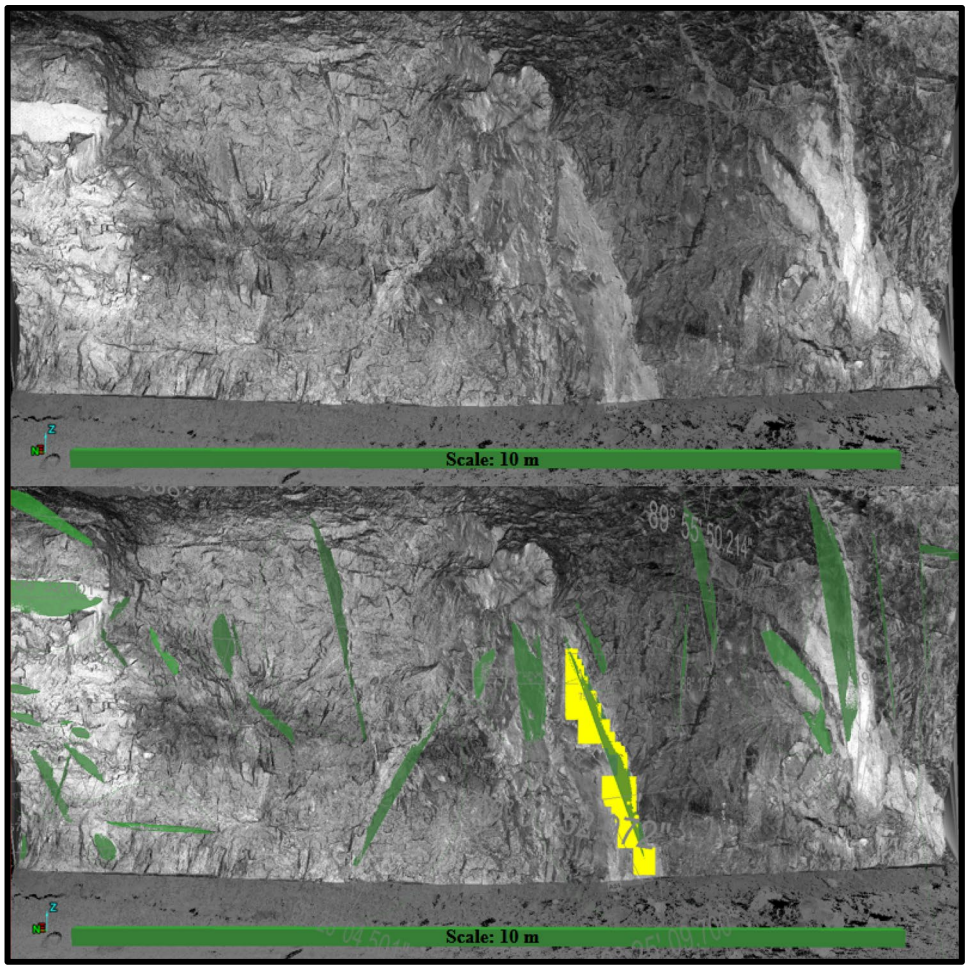


**Fig. 13** Discontinuity mapping from LiDAR scans in Maptek I-Site [14]

**Table 2** Statistical data for each joint set used to generate discrete fracture networks

| | Joint sets | | S1 | S2 | S3 | S4 (bedding) |
|---|---|---|---|---|---|---|
| **Parameters** | **Orientation** | **Dip (°)** | 88 | 68 | 75 | 29 |
| | | **Dip direction (°)** | 255 | 348 | 21 | 144 |
| | | **K (Fisher distribution)** | 103.9 | 102.4 | 69.5 | 197.3 |
| | **Size** | **Distribution** | Log-normal | Log-normal | Log-normal | Log-normal |
| | | **Mean** | 0.353 | 0.318 | 0.018 | 0.778 |
| | | **Standard deviation** | 0.659 | 0.772 | 0.749 | 0.934 |
| | **Density** | **$P_{32}$ (joint area/volume)** | 0.045 | 0.095 | 0.181 | 0.227 |

$P_{10}$ is defined as the number of fractures measured along scanlines [18]. The $P_{32}$ value is set in the numerical model such that the fractures are generated in the model yield the $P_{10}$ value equivalent to the one mapped in the field using virtual discontinuity mapping from LiDAR scans. Figure 14 shows the DFNs of different joint sets merged to form a combination of simulated fracture networks which was used to cut the Pillar-X model in all scenarios.

## 6 Results and Analysis

The numerical modeling analysis for the three scenarios was performed to observe the deterioration of the pillar with increasing stress levels. It should be noted that the stress levels are plotted versus the axial strain along the pillar. Since a constant velocity boundary was applied to the top and bottom surface planes of the pillar model, visualizing stress with axial strain would also indicate the

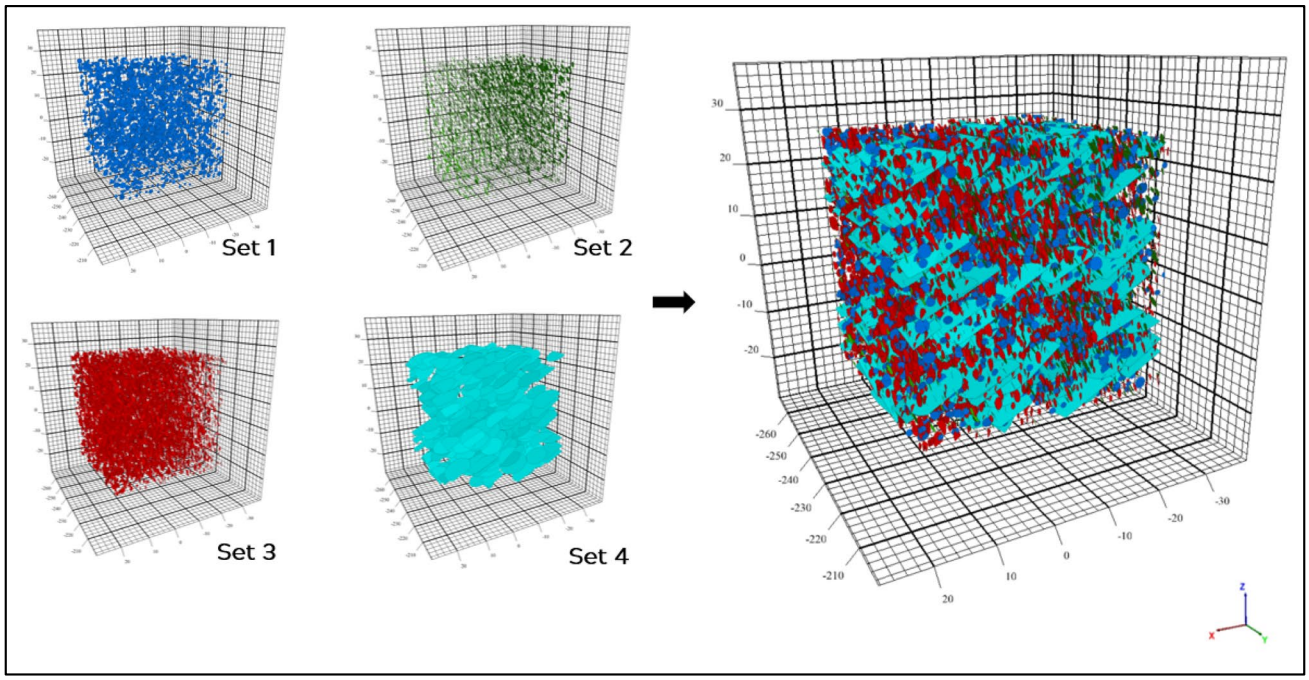


**Fig. 14** DFNs of different joint sets merged to form a combination fracture network in 3DEC

modulus of the rock mass with discontinuities. The analyses are explained below:

i. *Scenario 1* — In scenario 1, numerical modeling was performed to the original pillar model without the presence of karst voids in it. The pillar model was cut from the discrete fracture network as explained in the previous section. The model was then subjected to increasing stress levels until yielding occurs and ultimately failure is achieved. Figure 15 shows the deterioration of the pillar with increasing stress levels. It is observed that as the compressive stress increases, an increase in rock boulder failure and spalling from the sidewall occurs. The observed spalling is due to the increase in tensile stresses along the sidewall of the pillar. Also, major weakening occurs due to the simulated increase in compressive stresses. It is inferred that a combination of these stresses leads to the ultimate failure of the pillar rock mass yielding at its ultimate strength. Simulating a solid pillar model without karsts allows us to make a comparison as to what is the effect of the introduction of cavities in the pillar has on its strength. It is visible that the pillar fails when the applied stress magnitude reaches ~ 54 MPa. Even before the stress value reaches at failure level, at around ~ 43 MPa, the sidewall of the pillar looks to have significantly deteriorated.
ii. *Scenario 2* — Figure. 16 shows the condition of Pillar-X in scenario 2 with the increase in stresses. It shows the simulation of the pillar with the suggested karst voids. It is observed that the ground failure from the sidewall has increased in this scenario for the same stresses in scenario 1. Pillar-X yields and ultimately failure occurs at around 43 MPa. This shows that the strength of the pillar has reduced although not too much, but still proves that the presence of karst cavities reduces the pillar strength. The spike observed in the stress–strain curve is attributed to simulation error that may have been generated due to a massive rock block separating from the pillar.
iii. *Scenario 3* — Simulation of Pillar-X with the worst-case of assuming the biggest karst void is performed in scenario 3. Figure 17 shows that the breakage of material and spalling has increased significantly compared to other scenarios. With increasing stress levels, the pillar yields and fails at a highly reduced value of ~ 28 MPa. This suggests that with increasing karst void volume, the deterioration increases as the strength of the pillar decreases significantly.

## 7 Conclusions

This study simulates the presence of karst voids in a pillar in an underground limestone mine. Different results are achieved when testing the strength of Pillar-X in three different scenarios of varying karst cavity volume. The

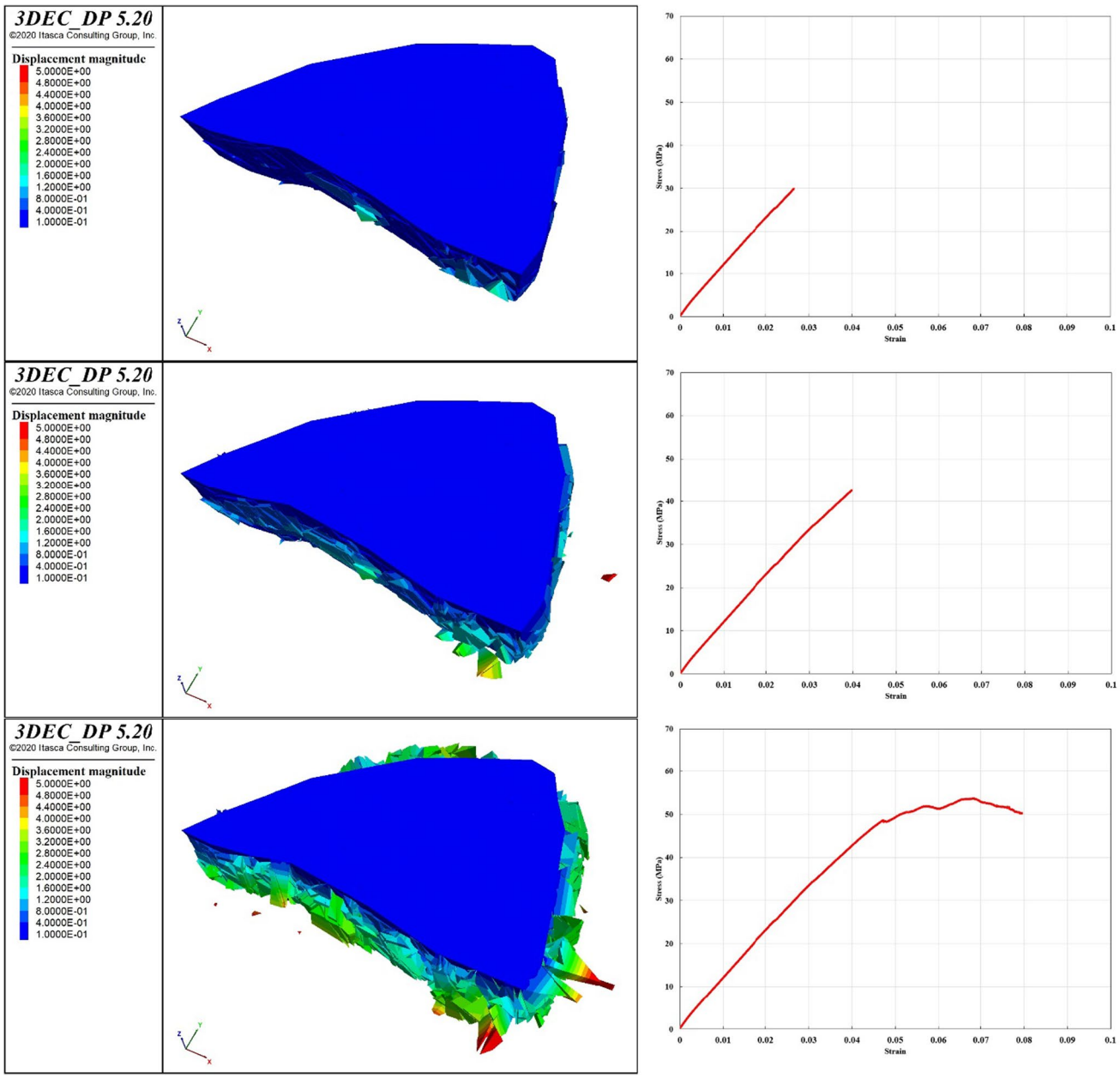


**Fig. 15** Deterioration phases of Pillar-X with increasing stress levels in scenario 1

miners in the case study mine have had many encounters with karst-related safety incidents during excavation operations. This study is important to design the pillar and headings for future mining operations and the use of numerical modeling to assess local stability with the presence of karsts. The following conclusions can be drawn from this study:

i. Karst-related safety incidents are quite common in stone mining operations. The karst voids, filled with rocky-clayey material, may interact with the immediate roof and fracture network resulting in ground collapse. This may endanger the safety of the mineworkers and mine machinery.
ii. To assess the strength of Pillar-X, different scenarios were simulated. The solid pillar with no karst voids failed at ~ 54 MPa showing the highest strength of all three scenarios. Stress was applied to the top and bottom face of the pillar in the form of constant velocity in 3DEC. Deterioration of the pillar was observed with increasing compressive stresses plotted against the axial strain.

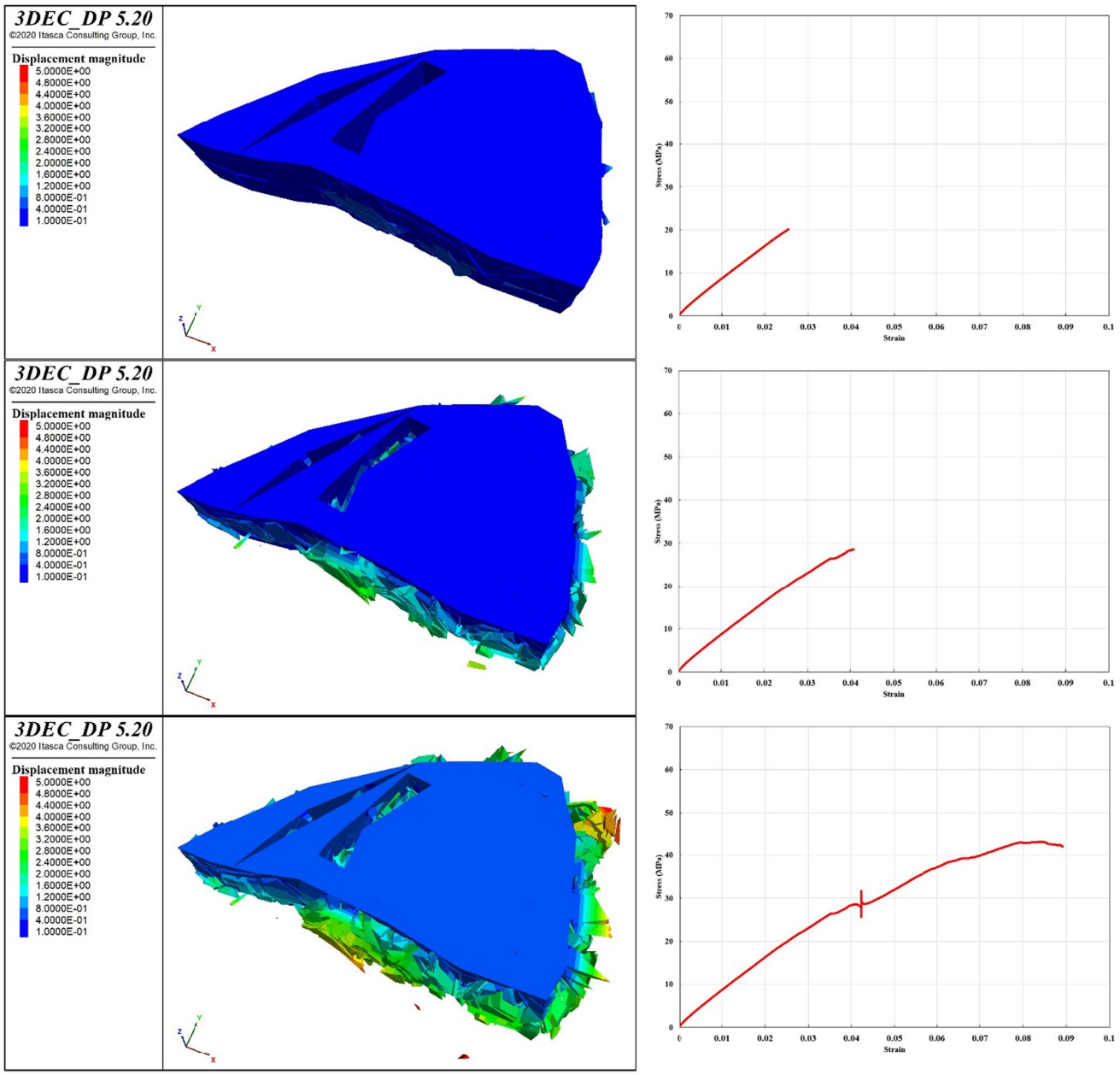


**Fig. 16** Deterioration phases of Pillar-X with increasing stress levels in scenario 2

iii. The pillar with the suggested karst voids in scenario 2 yielded and ultimately failed at ~ 43 MPa. It showed a reduced strength as compared to the original pillar in scenario 1 indicating a reduction in strength due to the presence of karst inside.

iv. The worst-case scenario with the biggest karst void showed the least strength of all the models. With a failure stress level of ~ 28 MPa, the pillar deteriorated too much as compared to the previous scenarios.

v. The numerical modeling study suggested that as the void volume inside the pillar increases, the ability of the pillar to withstand higher stresses decreases. Figure 18 shows a comparison of all the scenario models with increasing stress with time steps.

Concluding numerical modeling research to this study, which is published as a separate article, has been conducted at the case study mine. The study estimates the redistributed compressive stresses in and around the pillar to be in the range of ~5–8 MPa. Looking at the strength of the pillar scenarios, it may be inferred that despite the presence of karsts, the pillar can withhold higher stresses than the current stress

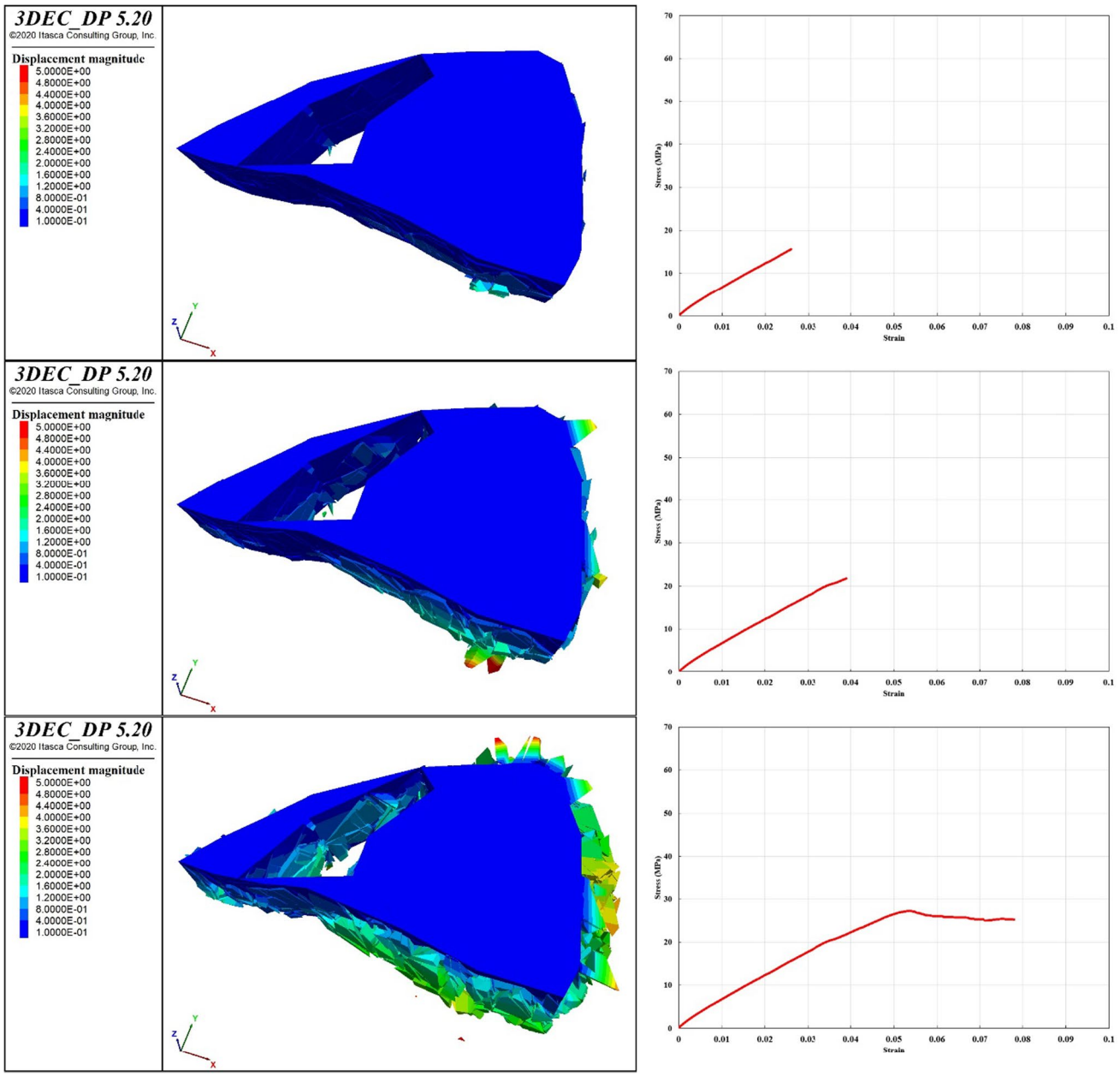


**Fig. 17** Deterioration phases of Pillar-X with increasing stress levels in scenario 3

condition. Although the mine management would not like to design the pillar within their desired Factor of Safety limit so that the stresses would not reach anywhere near the yielding point where substantial deterioration may occur. In this case, the numerical modeling allows picturizing the ground condition at the stress level at which the maximum limestone could be mined around the pillar without compromising the safety of the mine-workers or machinery.

## 8 Scope of the Study

This paper summarizes the numerical modeling analyses performed on the Pillar-X in a multi-level room-and-pillar underground limestone mine. Insufficient research exists to understand the impacts on pillar stability caused by the presence of karst voids. This study quantifies this effect in different scenarios, each with increasing the cavity volume

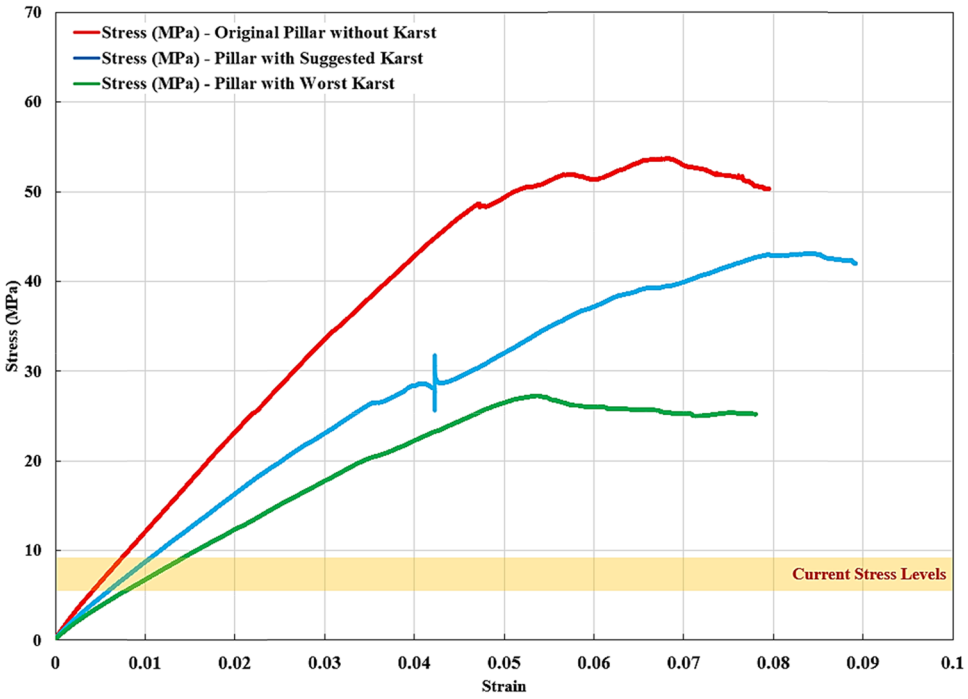


**Fig. 18** Increasing stress with time steps for all scenarios along with estimated stress levels in the pillar

to better understand the reduction in strength of a pillar with increasing compressive stresses. For this study, it is assumed that the compressive stress or vertical stress is imparted along the axis of the pillar, thus compressing the pillar. Even with the presence of the karst voids, the pillar could face higher stresses than the suggested current stress level of ~5–8 MPa existing in and around the pillar. Hence, it may be inferred that there is room for improvement regarding the pillar design. It could be concluded that more ore could have been taken out of the pillar without compromising its safety. The picturization of pillar deterioration with the increase in stresses allows us to decide the pillar strength at which the mine management would be comfortable with the pillar condition. And further improvements in design could be made until satisfaction is achieved with the pre-decided factor of safety of the pillar. The authors are currently working towards simulating models using different constitutive models to have a comprehensive idea about the plastic behavior of the rock mass. This would allow us to further refine the pillar design and compare the results of this study to another one where the plastic behavior of the rock mass dominates. Since the pillars and headings around Pillar-X were designed based on its width dimensions, optimizing material extraction could only be done while modifying the pillar along its axis. The authors suggest extracting the stopes on the subsequent levels, which were not excavated thus leaving the pillar with its shortened height. A separate study is underway to suggest appropriate modifications to the pillar given its strength and existing stress levels.

At higher depths, the redistributed stress acting on the pillars is highly likely to increase. In this case, the numerical model would be an effective tool to reconsider the current rectangular design of the pillars in the case study mine. Also, if any karst cavities are encountered, pillar or heading design could be varied and analyzed using 3DEC as a distinct element modeling tool to enclose the voids in the pillar while maintaining its stability. This study could also be important in helping with the secondary recovery from the remnant pillars in the mine to maximize ore extraction from the mine. Finally, when combined with karst-detection technologies such as probing or geophysical methods, numerical DEM could be effective to suggest any design changes while stoping and/or advancing while maintaining local as well as global mine stability.

**Acknowledgements** The authors would like to thank Dr. James Hazzard and Itasca Consulting Group for their support and guidance during this study.

**Author Contribution** Not applicable.

**Funding** This work is funded by the National Institute for Occupational Safety and Health (NIOSH) Mining Program under Contract No. 200–2016-91300. Views expressed here are those of the authors and do not necessarily represent those of any funding source.

**Data Availability** Not applicable.

**Code Availability** Not applicable.

## Declarations

**Ethics Approval** Not applicable.

**Consent to Participate** Not applicable.

**Consent for Publication** Not applicable.

**Conflict of Interest** The authors declare no competing interests.

## References


1. Kuniansky EL, Weary DJ, Kaufmann JE (2016) The current status of mapping karst areas and availability of public sinkhole-risk resources in karst terrains of the United States. J Hydrogeol 24(3):613–624
2. Gongyu Li, Wanfang Z (1999) Sinkholes in karst mining areas in China and some methods of prevention. J Engineering Geology 52(1–2):45–50
3. Andriani GF, Parise M (2017) Applying rock mass classifications to carbonate rocks for engineering purposes with a new approach using the rock engineering system. J Rock Mech Geotech Eng 9(2):364–369
4. Baggett JG (2019). A Study ofGround Penetrating Radar Methods in an Underground Stone Mine to Improve Ground Control (Master Thesis, Virginia Tech).
5. Davis JL, Annan A (1989) Ground-penetrating radar for high-resolution mapping of soil and rock stratigraphy. Geophysical prospecting Res 37(5):531–551
6. Grasmueck M (1996) 3-D ground-penetrating radar applied to fracture imaging in gneiss. Geophys 61(4):1050–1064
7. Annan AP, Davis JL (1976) Impulse radar sounding in permafrost. Radio Sci 11(4):383–394
8. Esterhuizen GS, Dolinar DR, Ellenberger JL (2011) Pillar strength in underground stone mines in the United States. Int J Rock Mech Min Sci 48(1):42–50
9. Esterhuizen GS, Dolinar DR., Ellenberger JL, Prosser LJ (2011) Pillar and roof span design guidelines for underground stone mines
10. Cacciari PP, Futai MM (2016) Mapping and characterization of rock discontinuities in a tunnel using 3D terrestrial laser scanning. Bull Eng Geol Env 75(1):223–237
11. Esterhuizen GS, Dolinar DR, Ellenberger JL (2008) Pillar strength and design methodology for stone mines. In Proceedings of the 27th international conference on ground control in mining. Morgantown WV: West Virginia University (241–253)
12. Iannacchione AT (1999) Pillar design issues for underground stone mines.
13. Bandis S, Lumsden A, Barton N (1983) Fundamentals of rock joint deformation. Int J Rock Mech Min Sci Geomechanics 20(6):249–268. Pergamon
14. Monsalve JJ, Baggett JG, Soni A, Ripepi N, Hazzard J (2019) Stability analysis of an underground limestone mine using terrestrial laser scanning with stochastic discrete element modeling. In 53rd US Rock Mechanics/Geomechanics Symposium. OnePetro
15. McDowell RC, Schultz AP (1990) Structural and stratigraphic framework of the Giles County area, a part of the Appalachian Basin of Virginia and West Virginia (No. 1839-E)
16. 3DEC Version 5.2 (2019) User's manual. Itasca Consulting Group, Minneapolis, Minnesota
17. Pierce M (2017) An introduction to random disk discrete fracture network (DFN) for civil and mining engineering applications. ARMA e-Newsletter 20:3–8
18. Miyoshi T, Elmo D, Rogers S (2018) Influence of data analysis when exploiting DFN model representation in the application of rock mass classification systems. J Rock Mechanics Geotech Eng 10(6):1046–1062